Gaussian deformations in graphene ribbons: Flowers and confinement

R. Carrillo-Bastos,[1,2,3,*] D. Faria,[4] A. Latgé,[4] F. Mireles,[2] and N. Sandler[3]

[1]*Centro de Investigación Científica y de Educación Superior de Ensenada, Apado. Postal 360, 22800 Ensenada, Baja California, México*
[2]*Universidad Nacional Autónoma de México, Apdo. Postal 14, 22800 Ensenada, Baja California, México*
[3]*Ohio University, Athens, Ohio 45701-2979, USA*
[4]*Universidade Federal Fluminense, Niterói, Avenida Litorânea sn, 24210-340 RJ, Brasil*

The coupling of geometrical and electronic properties is a promising venue to engineer conduction properties in graphene. Confinement added to strain allows for interplay of different transport mechanisms with potential device applications. To investigate strain signatures on transport in confined geometries, we focus on graphene nanoribbons (GNRs) with circularly symmetric deformations. In particular, we study GNRs with an inhomogeneous out-of-plane Gaussian deformation, connected to reservoirs. We observe an enhancement of the density of states in the deformed region, accompanied with a decrease in the conductance, signaling the presence of confined states. The local density of states exhibits a sixfold symmetric structure with an oscillating sublattice occupation asymmetry that persists for a wide range of energy and model parameters.

Graphene nanoribbons (GNRs) constitute a viable way to exploit the extraordinary electronic transport properties of graphene [1]. The rich combination of peculiar properties due to confinement and potential technological applications have guided research on nanoribbons since the pioneering studies by Nakada *et al.* [2]. With improved control of growth and manipulation techniques of graphene flakes and carbon nanotubes [3,4], experimental studies focused on different aspects of the physics displayed in these reduced geometries. Original works confirmed the appearance of gaps due to confinement [5,6], and later experiments demonstrated the stability of zigzag terminated structures [7,8]. Further studies focused on issues such as tailored edge terminations [9,10], atomic scale control of electric contacts [11], and transport properties at high biases [5]. Furthermore, it was recently reported that ribbons grown epitaxially on SiC can stand ballistic transport on length scales greater than 10 μm [12], a finding very relevant for electronic applications. The fast pace of experimental studies is stimulated—and accompanied—by a vast amount of theoretical work predicting a wide variety of phenomena from localized magnetic properties at the edges, to exotic topological phases [13,14]. Recently, studies have begun to address the effect of strain in transport properties of confined systems and ribbon junctions.

Strain in graphene has been the topic of a large number of theoretical works [15–24] aimed at understanding the effects of controlled deformations on electronic properties. As charge carriers near the neutrality point behave as massless Dirac particles moving on a deformed lattice, many aspects of fundamental physics involved in the dynamics of such a system can be studied in great detail on current settings. Experimental works have analyzed different aspects of strain on graphene: from the initial measurements of its intrinsic strength and elastic properties [25] to the more recent identification of pseudo-Landau levels (LL) associated with

gigantic pseudomagnetic fields produced in highly strained samples [26]. These achievements are accompanied by the development of devices such as strain based graphene sensors [27] and piezoelectrics, among others, giving rise to the nascent field of straintronics [28].

Although a good degree of understanding of homogeneous strain has been achieved in recent years, the role of nonuniform strain, and in particular, in confined open geometries, still remains unexplored. The purpose of this paper is to provide insight into this issue by studying equilibrium and transport properties of strained nanoribbons with armchair and zigzag edges connected to reservoirs. Most of the theoretical work on transport in deformed graphene has focused on uniaxial strain [29–33], with centrosymmetric deformations being analyzed in closed geometries [34–37] or in open systems within the Born approximation [38]. We focus here on strain produced by a centrosymmetric Gaussian (out-of-plane) deformation located at the center of the nanoribbon as shown in Fig. 1. These deformations can serve as a model for a load in a membrane [21], ripples in free standing graphene [39], or Gaussian patterns in substrates [40]. They have been already produced on suitable substrates [41] and also with STM methods [42,43]. Two main results emerge from this study: (i) These deformations confine states within the ribbon, with the consequent decrease of the conductance and corresponding peaks appearing in the associated density of states (DOS); and (ii) the local density of states (LDOS) exhibits a sixfold symmetry pattern that we refer to as the "flower," with sublattice polarization in each sector (or "petal"). These results, independent of the crystalline orientation, exhibit interesting features discussed below, and are analogous to the proposed Dirac fermion confinement with real magnetic fields [44]. Our study focuses on transport mechanisms different from LL-assisted tunneling [45] that has been proposed to explain recent experimental [26] and theoretical results obtained for strained ribbons [31,46].

Model for GNRs with Gaussian Deformation. We consider a nanoribbon with N_x (N_y) sites on the horizontal (vertical)
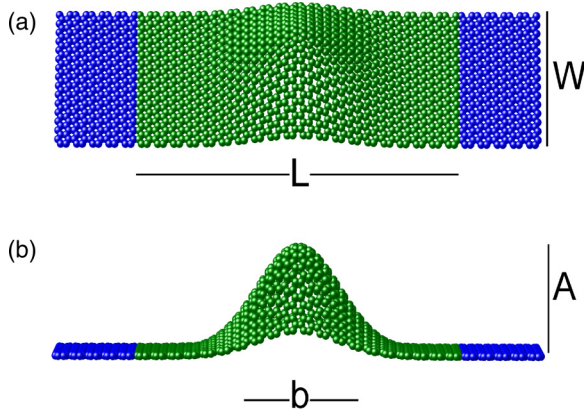
---
*[*]nomarcb@hotmail.com

FIG. 1. (Color online) Schematic representation of deformed GNRs (width W and length L) connected to leads with a Gaussian deformation (amplitude A and dispersion b).

direction, connected to infinite graphene leads (see Fig. 1) modeled by the tight-binding Hamiltonian:

$$H = \sum_{\langle i,j \rangle} t_{ij} c_i^\dagger c_j + \sum_{\langle i,k_l \rangle} t_0 c_i^\dagger c_{k_l} + \sum_{\langle i,k_r \rangle} t_0 c_i^\dagger c_{k_r}. \quad (1)$$

Here the first term refers to the central (deformed) system, while the second and third terms describe the connection to the reservoirs, with the indices k_l, k_r running over the sites of the left and right leads. $c_i^\dagger$ (c_i) is the creation (annihilation) field operator in the ith site, t_{ij} is the nearest-neighbor hopping energy, and we take $t_0 = -2.8$ eV as the hopping parameter in the absence of deformation. The strain introduced by the Gaussian deformation modifies t_{ij} as $t_{ij} = t_0 \Delta_{ij}$ with $\Delta_{ij} = e^{-\beta(l_{ij}/a - 1)}$.

The interatomic distance in unstrained graphene is $a = 1.42$ Å, and the coefficient $\beta = |\frac{\partial \log t_o}{\partial \log a}| = 3.37$. The distance $l_{ij} = \frac{1}{a}(a^2 + \varepsilon_{xx} x_{ij}^2 + \varepsilon_{yy} y_{ij}^2 + 2\varepsilon_{xy} x_{ij} y_{ij})$ is given by the strain tensor $\varepsilon_{\mu\nu} = \frac{1}{2}(\partial_\nu u_\mu + \partial_\mu u_\nu + \partial_\mu h \partial_\nu h)$, characterized

by the in- and out-of-plane deformation u_ν and h, respectively [47]. The out-of-plane deformation

$$h(x_i, y_i) = A e^{-\frac{(x_i - x_0)^2 + (y_i - y_0)^2}{b^2}} \quad (2)$$

has center at $[x_0; y_0]$ [we use $(x_0 = L/2, y_0 = W/2)$ for the center of the ribbon], and A and b describe its amplitude and width, respectively. The hopping modification can be understood as a gauge field [48]. For a Gaussian deformation this field has a threefold spatial distribution with different profiles for zigzag and armchair crystal directions [34,35]. Notice that the bump also produces a deformation potential, akin to a local chemical potential [48], whose effects have not been included in the results showed below. Consequences of its presence are discussed in detail in the Supplemental Materials [49], where it is shown that due to its axial symmetry, it does not affect the main findings of this paper. Equation (1) is used to obtain the retarded Green's function by recursive methods. Self-energies $\Sigma_{r,l}$ associated with the leads, are calculated by standard decimation methods. Finally, the conductance is calculated via the Landauer formula and Fisher-Lee relation [50].

Conductance and DOS. The conductance and DOS for strained ribbons with armchair (AGNR) and zigzag (ZGNR) terminations are shown in Fig. 2 for deformations with varying amplitude A and fixed width b. In both cases the position of the deformation is at the center of one hexagonal cell. The data is shown for AGNR with $L = 30.7$ nm and $W = 30.0$ nm (288×245 atomic sites) and for ZGNR with $L = 27.4$ nm and $W = 25.8$ nm (224×244 atomic sites). Similar results were observed with different ribbon sizes and positions of the Gaussian center (within a radius of ~ 0.2 nm). For all panels, the dashed (black) lines correspond to results in the absence of the deformation and continuous (color online) lines to different values of A.

Conductance results are shown in Figs. 2(a) and 2(b) for AGNR and ZGNR, respectively. Both ribbons are metallic and the conductance exhibits the standard stepwise behavior for the
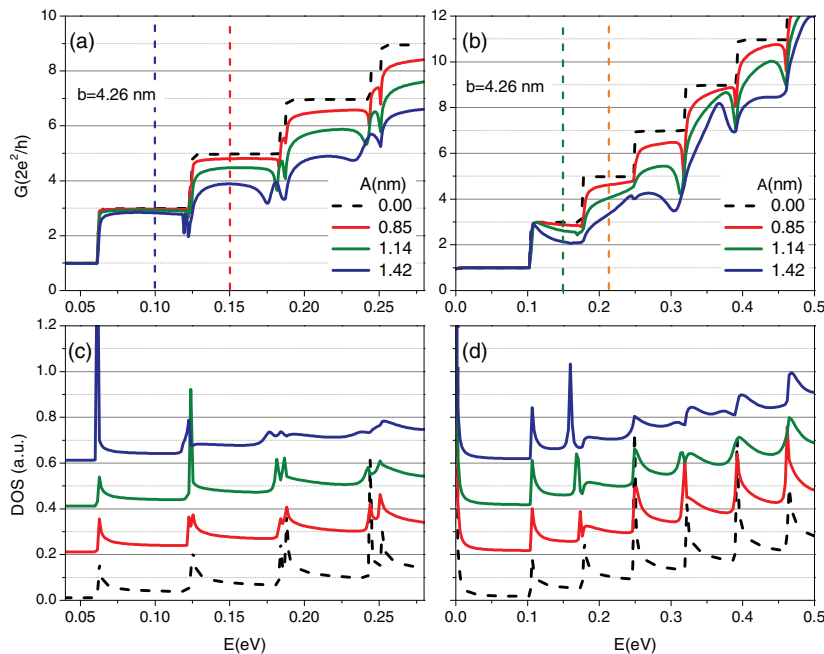

FIG. 2. (Color online) Conductance and DOS for: (a) and (c) AGNR, and (b) and (d) ZGNR for different values of A, and fixed width $b = 4.3$ nm, corresponding to strains of 4%, 7%, and 11%, respectively. Black dashed lines corresponds to the nondeformed ribbon. Data for deformed DOS have been shifted for clarity. Vertical lines indicate energies values at which LDOS plots are shown in Fig. 4.
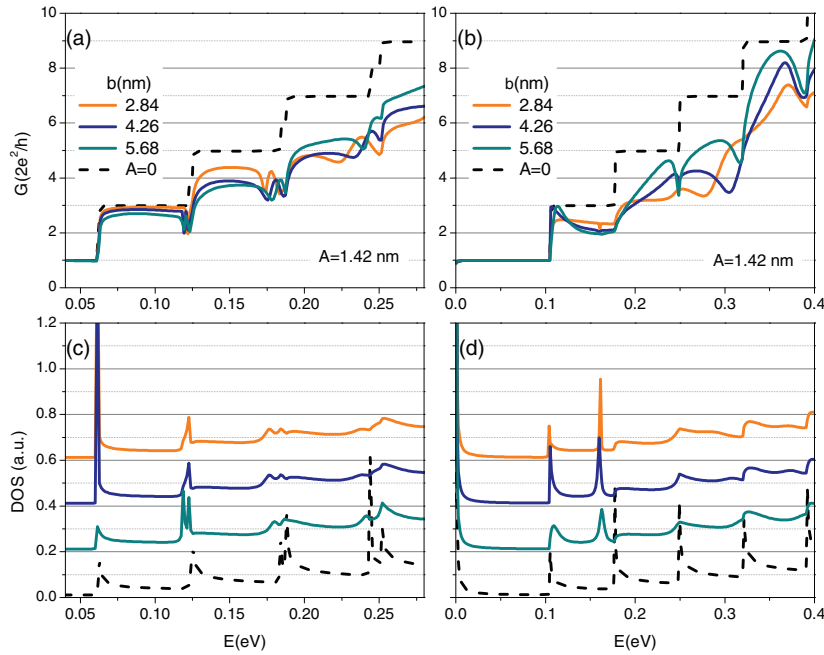
FIG. 3. (Color online) Conductance and DOS for: (a) and (c) AGNR, and (b) and (d) ZGNR for AGNR, different values of b, and fixed amplitude $A = 1.42$ nm, corresponding to strains of 7%, 11%, and 25%, respectively. The (black) dashed line corresponds to the nondeformed ribbon. Data for deformed DOS have been shifted for clarity.

unstrained case (black dashed lines). For both terminations, the zero plateau is not modified by the Gaussian deformation, in contrast with results obtained with uniaxial in-plane strained junctions [30]. As A increases, the value of the conductance decreases for nonzero plateaus. Note that the conductance for ZGNR and AGNR ribbons exhibit different profiles. These differences may be caused by the distinct orientations of the pseudomagnetic field space distributions with respect to the position of the leads. These distributions are 90° rotated with respect to each other resulting in different scattering cross sections as shown by perturbation theory calculations on the continuum model [38]. A common feature for both ribbons is the appearance of pronounced minima at the step-to-step transition, which have been observed in other systems, and are associated with interband mixing favored by the presence of perturbations [51].

Figures 2(c) and 2(d) show results for the corresponding DOS. The DOS curve for ZGNR shows the peak at zero energy corresponding to edge states that remains largely unaffected by the deformations from 4% up to a level of 11% strain. As the deformation is turned on, for both terminations, sharp peaks appear at lower energies followed by local minima. These minima are followed by raising features precisely at the energy values corresponding to the van Hove singularities in the absence of deformation. Thus, peaks in the undeformed system shift spectral weight to lower energy peaks. These new peaks—in contrast to the original ones—are symmetric, a fact more evident for ZGNR (see, for example, the third peak). This effect is accompanied by a decrease in height of higher energy peaks and a slow smoothening of the DOS. Notice that states in the newly formed low-energy DOS peaks (produced by inhomogeneous pseudomagnetic field), do not generate additional contributions to the conductance. This indicates an incipient localization at the deformation region, in contrast with previous studies where extended regions with constant pseudomagnetic field generate pseudo LLs available for tunneling assisted transport [31,45].

Figure 3 shows similar results for a deformation with constant amplitude A and variable width b. For both ribbon terminations, an increase in the curvature of the deformation (decreasing the value of b) results in a deterioration of the conductance and confined states. We find that the energy of the newly confined level decreases quadratically with the aspect ratio (A/b), a result predicted in the continuum description (Dirac) by perturbation theory and confirmed by scattering calculations [52].

LDOS and Pseudospin Polarization. Nonhomogeneous strain has profound effects on the space distribution of the DOS. An analysis of the LDOS reveals a well-defined pattern with a 60° symmetry, i.e., the petals of the flower structure. Figure 4 presents typical LDOS structures obtained for AGRN and ZGNR at energies marked by vertical lines in Fig. 2. We have confirmed that this structure persists for a wide energy range and deformation parameter values (not shown). Similar patterns have been obtained in models for closed systems [21–23,34,36]. Notice that the structures for ZGNR and AGNR are rotated 90° relative to each other, following the spatial distribution of the pseudomagnetic field [35].

Figure 5 shows a zoom-in of one particular structure, for a ZGNR. The undeformed graphene lattice is represented by up- and downside triangles (distinguishing sublattices). The black dot represents the maximum height of the Gaussian bump that is centered in a maximum symmetry position in the ribbon. The values for sublattice occupancy alternates from petal to petal, signaling a characteristic sublattice asymmetry or pseudospin polarization with threefold symmetry. Such structure could be linked to a geometrical description of the microscopic model as realized in Ref. [23]. Similar effects, with chiral states within the zero LL [53], were obtained in models of Dirac fermions with magnetic field in bounded regions [54].

In Figs. 5(b) and 5(c) we show values of LDOS on each sublattice. Figure 5(b) exhibits the largest occupancies (darker regions) at the bottom petals, while the contrary occurs in Fig. 5(c). Notice that zigzag boundaries naturally introduce
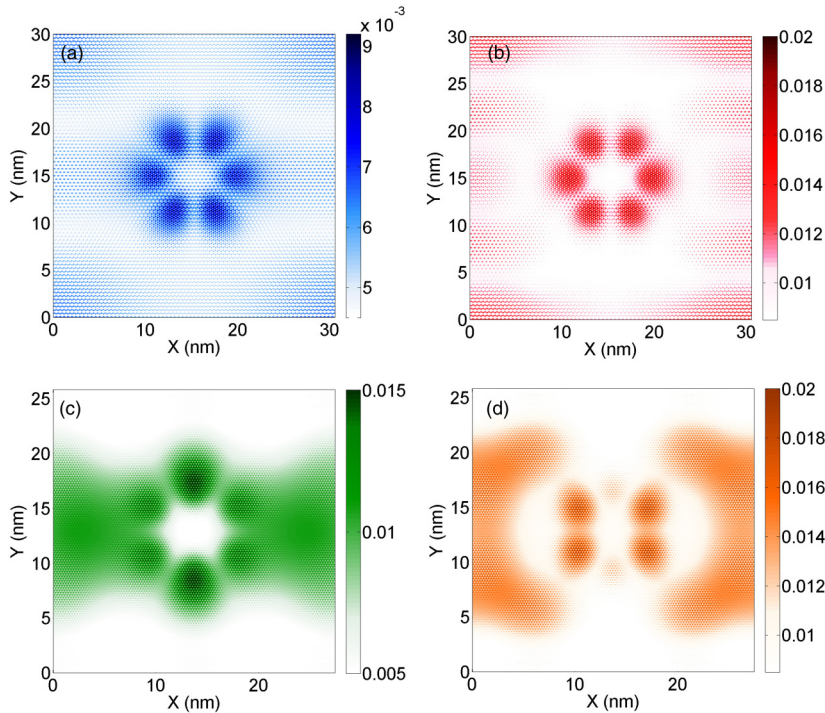
FIG. 4. (Color online) LDOS for: (a) and (b) AGNR, and (c) and (d) ZGNR with deformation amplitude $A = 1.42$ nm and $b = 4.3$ nm at energies shown in Fig. 2 (vertical dashed lines): (a) (blue) $E = 0.1$ eV, (b) (red) $E = 0.15$ eV, (c) (green) $E = 0.15$ eV, and (d) (orange) $E = 0.21$ eV. Scales (a.u.) in each plot are optimized to exhibit areas with higher density of states.

a difference in sublattice occupancies due to the different sublattice terminations at the top and bottom edges. These
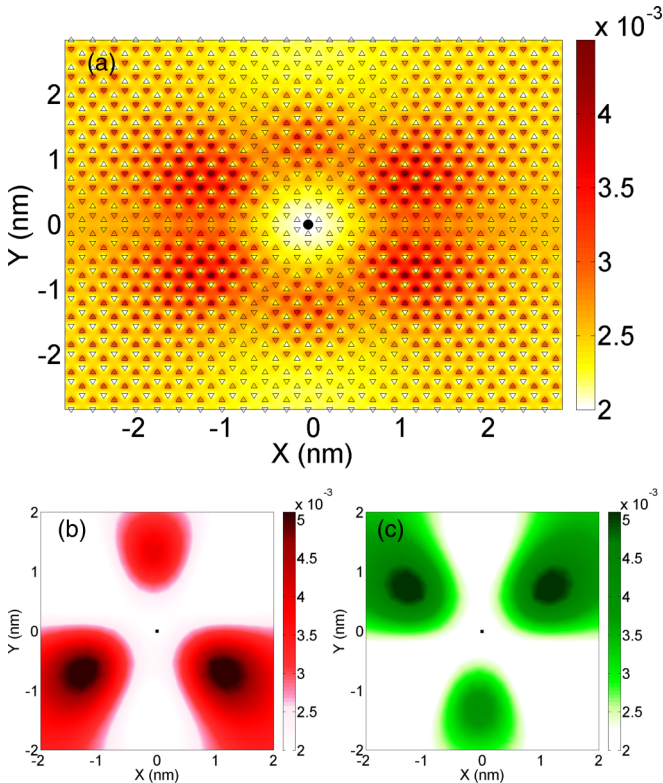

FIG. 5. (Color online) (a) LDOS (a.u.) for ZGNR of width $W = 25.8$ nm, and length $L = 27.3$ nm, with Gaussian deformation of amplitude $A = 0.7$ nm and $b = 1.4$ nm, plotted at energy $E = 0.042$ eV. Atomic positions of undeformed graphene lattice marked with up- and downside triangles for each sublattice. The center of the Gaussian is marked with the black circle. (b) Sublattice A. (c) Sublattice B.

differences, due to "edge states," are predicted to be localized at the edges, however for finite systems the amplitude of edge states decays inside the ribbon [55]. It is thus natural to interpret the "darker regions" breaking the three-petal symmetry as a consequence of edge states in ZGNR. To confirm these hypothesis we carried out calculations for AGNR that reveal the same alternate pattern for sublattice occupancy [49]. In these systems the whole flower structure possesses dark regions in the petals appearing closer to the contacts to reservoirs. Although the leads are modeled as perfect graphene lattices, the absence of the deformation in the reservoirs could create an effective boundary condition at the contact, thus representing potentially a zigzag boundary. The presence of these developing edge states at the contacts could enhance the sublattice occupancy in certain petals. Calculations carried out in larger AGRN with deformation amplitudes vanishing before reaching contact regions (thus eliminating a "zigzag boundary"), show that the distribution of the highest occupied petals becomes energy dependent with a persistence asymmetry between petals. However, this asymmetry decreases with increasing AGNR width, suggesting a strong dependence on the underlying LDOS for the undeformed system.

Further calculations reveal that pseudospin polarization appears in a wide range of energies, and deformation parameters, indicating a robust effect that persists in the presence of external magnetic fields [52]. Note that this local breaking of sublattice symmetry (local breaking of inversion symmetry) does not open a gap as evidenced by the finite conductance. Although several theory studies have predicted sublattice asymmetry features in the LDOS [22,23,34,56], these appear to have been overlooked in STM experimental studies [42,57,58] since no explicit connection with centrosymmetric deformations have been made. Our results, showing a peculiar sequential pattern for sublattice occupation, provide a possible

test for the origin of the observed asymmetries that could be tested in current experimental settings [59].

Conclusions. In closing, we present a study of conductance of strained ribbons with Gaussian deformations that produce inhomogeneous pseudomagnetic fields at every length scale. In this system there are no Landau levels available for transport but instead there are bound states that concentrate in the region where the pseudomagnetic field acquires its maximum value. We provide a real space description of the location and symmetry of these states that exhibit a sublattice occupation alternation of $60°$, associated with a local pseudospin polarization in the continuum Dirac (low-energy) description. These results are largely independent of lattice orientation.

All these effects are within reach of current experiments and open the exciting possibility to design deformations for desired electronic confinement.

---

[1] A. H. Castro Neto, F. Guinea, N. M. R. Peres, K. S. Novoselov, and A. K. Geim, Rev. Mod. Phys. **81**, 109 (2009).

[2] K. Nakada, M. Fujita, G. Dresselhaus, and M. S. Dresselhaus, Phys. Rev. B **54**, 17954 (1996).

[3] L. Ma, J. Wang, and F. Ding, Chem. Phys. Chem. **14**, 47 (2013).

[4] C. Tao, L. Jiao, O. V. Yazyev, Y.-C. Chen, J. Feng, X. Zhang, R. B. Capaz, J. M. Tour, A. Zettl, S. G. Louie, H. Dai, and M. F. Crommie, Nat. Phys. **7**, 616 (2011).

[5] M. Y. Han, B. Özyilmaz, Y. Zhang, and P. Kim, Phys. Rev. Lett. **98**, 206805 (2007).

[6] Y.-M. Lin, V. Perebeinos, Z. Chen, and P. Avouris, Phys. Rev. B **78**, 161409 (2008).

[7] X. Jia, M. Hofmann, V. Meunier, B. G. Sumpter, J. Campos-Delgado, J. M. Romo-Herrera, H. Son, Y.-P. Hsieh, A. Reina, J. Kong, M. Terrones, and M. S. Dresselhaus, Science **323**, 1701 (2009).

[8] Ç. O. Girit, J. C. Meyer, R. Erni, M. D. Rossell, C. Kisielowski, L. Yang, C.-H. Park, M. F. Crommie, M. L. Cohen, S. G. Louie, and A. Zettl, Science **323**, 1705 (2009).

[9] A. Chuvilin, E. Bichoutskaia, M. C. Gimenez-Lopez, T. W. Chamberlain, G. A. Rance, N. Kuganathan, J. Biskupek, U. Kaiser, and A. N. Kholobystov, Nat. Mater. **10**, 687 (2011).

[10] X. Zhang, O. V. Yazyev, J. Feng, L. Xie, C. Tao, Y. C. Chen, L. Jiao, Z. Pedramrazi, A. Zettl, S. G. Louie, H. Dai, and M. F. Crommie, ACS Nano **7**, 198 (2013).

[11] J. van der Lit, M. P. Boneschanscher, D. Vanmaekelbergh, M. Ijäs, A. Uppstu, M. Ervasti, A. Harju, P. Liljeroth, and I. Swart, Nat. Commun. **4**, 2023 (2013).

[12] J. Baringhaus, M. Ruan, F. Edler, A. Tejeda, M. Sicot, A. Taleb-Ibrahimi, A.-P. Li, Z. Jiang, E. H. Conrad, C. Berger, C. Tegenkamp, and W. A. de Heer, Nature (London) **506**, 349 (2014).

[13] O. Yazyev, Acc. Chem. Res. **46**, 2319 (2013).

[14] J. J. Palacios, J. Fernández-Rossier, L. Brey, and H. A. Fertig, Semicond. Sci. Technol. **25**, 033003 (2010).

[15] F. de Juan, A. Cortijo, and M. A. H. Vozmediano, Phys. Rev. B **76**, 165409 (2007).

[16] F. Guinea, M. I. Katsnelson, and A. K. Geim, Nat. Phys. **6**, 30 (2009).

[17] V. M. Pereira and A. H. Castro Neto, Phys. Rev. Lett. **103**, 046801 (2009).

[18] T. Low, F. Guinea, and M. I. Katsnelson, Phys. Rev. B **83**, 195436 (2011).

[19] F. de Juan, M. Sturla, and M. A. H. Vozmediano, Phys. Rev. Lett. **108**, 227205 (2012).

[20] J. L. Mañes, F. de Juan, M. Sturla, and M. A. H. Vozmediano, Phys. Rev. B **88**, 155405 (2013).

[21] J. V. Sloan, A. A. Pacheco Sanjuan, Z. Wang, C. Horvath, and S. Barraza-Lopez, Phys. Rev. B **87**, 155436 (2013).

[22] S. Barraza-Lopez, A. A. Pacheco Sanjuan, Z. Wang, and M. Vanević, Solid State Commun. **166**, 70 (2013).

[23] A. A. Pacheco Sanjuan, Z. Wang, H. Pour Imani, M. Vanević, and S. Barraza-Lopez, Phys. Rev. B **89**, 121403 (2014).

[24] M. Oliva-Leyva and G. G. Naumis, Phys. Rev. B **88**, 085430 (2013).

[25] C. Lee, X. Wei, J. W. Kysar, and J. Hone, Science **321**, 385 (2008).

[26] N. Levy, S. A. Burke, K. L. Meaker, M. Panlasigui, A. Zettl, F. Guinea, A. H. C. Neto, and M. F. Crommie, Science **329**, 544 (2010).

[27] S.-H. Bae, Y. Lee, B. K. Sharma, H.-J. Lee, J.-H. Kim, and J.-H. Ahn, Carbon **51**, 236 (2013).

[28] M. T. Ong and E. J. Reed, ACS Nano **6**, 1387 (2012).

[29] V. M. Pereira, A. H. Castro Neto, and N. M. R. Peres, Phys. Rev. B **80**, 045401 (2009).

[30] D. A. Bahamon and V. M. Pereira, Phys. Rev. B **88**, 195416 (2013).

[31] D. A. Gradinar, M. Mucha-Kruczyński, H. Schomerus, and V. I. Fal'ko, Phys. Rev. Lett. **110**, 266801 (2013).

[32] E. Prada, P. San-Jose, G. León, M. M. Fogler, and F. Guinea, Phys. Rev. B **81**, 161402 (2010).

[33] M. M. Fogler, F. Guinea, and M. I. Katsnelson, Phys. Rev. Lett. **101**, 226804 (2008).

[34] D. Moldovan, M. Ramezani Masir, and F. M. Peeters, Phys. Rev. B **88**, 035446 (2013).

[35] D. Faria, A. Latgé, S. E. Ulloa, and N. Sandler, Phys. Rev. B **87**, 241403 (2013).

[36] G. M. M. Wakker, R. P. Tiwari, and M. Blaauboer, Phys. Rev. B **84**, 195427 (2011).

[37] K.-J. Kim, Y. M. Blanter, and K.-H. Ahn, Phys. Rev. B **84**, 081401 (2011).

[38] M. Yang, Y. Cui, R.-Q. Wang, and H.-B. Zhao, J. Appl. Phys. **112**, 073710 (2012).

[39] H. Wang and M. Upmanyu, Phys. Rev. B **86**, 205411 (2012).

[40] S. Viola Kusminskiy, D. K. Campbell, A. H. Castro Neto, and F. Guinea, Phys. Rev. B **83**, 165405 (2011).

[41] T. Georgiou, L. Britnell, P. Blake, R. V. Gorbachev, A. Gholinia, A. K. Geim, C. Casiraghi, and K. S. Novoselov, Appl. Phys. Lett. **99**, 093103 (2011).

[42] T. Mashoff, M. Pratzer, V. Geringer, T. J. Echtermeyer, M. C. Lemme, M. Liebmann, and M. Morgenstern, Nano Lett. **10**, 461 (2010).

[43] N. N. Klimov, S. Jung, S. Zhu, T. Li, C. A. Wright, S. D. Solares, D. B. Newell, N. B. Zhitenev, and J. A. Stroscio, Science **336**, 1557 (2012).

[44] A. De Martino, L. Dell'Anna, and R. Egger, Phys. Rev. Lett. **98**, 066802 (2007).

[45] Z. Qi, D. A. Bahamon, V. M. Pereira, H. S. Park, D. K. Campbell, and A. H. C. Neto, Nano Lett. **13**, 2692 (2013).

[46] M. Mucha-Kruczynski and V. I. Fal'ko, Solid State Commun. **152**, 1442 (2012).

[47] L. Landau and E. M. Lifshitz, *Theory of Elasticity (Volumen 7 of A Course of Theoretical Physics)* (Pergamon, Cambridge, 1970).

[48] H. Suzuura and T. Ando, Phys. Rev. B **65**, 235412 (2002).

[49] See Supplemental Material at http://link.aps.org/supplemental/10.1103/PhysRevB.90.041411 for detail analysis of the effects of the deformation potential .

[50] C. H. Lewenkopf and E. R. Mucciolo, J. Comput. Electron. **12**, 203 (2013).

[51] P. F. Bagwell, Phys. Rev. B **41**, 10354 (1990).

[52] M. Schneider, D. Faria, S. V. Kusminskiy, and N. Sandler (to be published).

[53] M. O. Goerbig, Rev. Mod. Phys. **83**, 1193 (2011).

[54] A. de Martino and R. Egger, Semicond. Sci. Technol. **25**, 034006 (2010).

[55] M. Fujita, K. Wakabayashi, K. Nakada, and K. Kusakabe, J. Phys. Soc. Jpn. **65**, 1920 (1996).

[56] M. Neek-Amal, L. Covaci, K. Shakouri, and F. M. Peeters, Phys. Rev. B **88**, 115428 (2013).

[57] K. Xu, P. Cao, and J. R. Heath, Nano Lett. **12**, 4446 (2009).

[58] S. A. Burke and M. Crommie (private communication).

[59] A. Georgi and M. Morgenstern (private communication).